

## Elliptical Galaxy Cooling Flows

Joel N. Bregman<sup>1</sup> and Alex E. Athey<sup>2</sup>

<sup>1</sup> *University of Michigan*

<sup>2</sup> *Carnegie Observatories*

For individual elliptical galaxies, the cooling flow model has the gas originating from stellar mass loss, subsequently becoming thermalized to the stellar velocity dispersion temperature, then cooling and falling into the central region. Supernova can modify this picture by heating the gas sufficiently to produce a galactic wind rather than a cooling flow. It should be possible to identify the signatures of these different stages using multifrequency observations. The stellar mass has been detected by the mid-infrared excess found with ISO-Cam, which is caused by silicate emission from the mass loss of giant stars. The magnitude of this emission, due to an ensemble of stars, is consistent with theoretical expectations, typically  $0.1\text{--}1 M_{\odot} \text{ yr}^{-1}$  for the nearby elliptical galaxies studied.

A sample of 37 ellipticals were studied with the Chandra observatory, where one can finally separate the X-ray point sources from the diffuse gaseous emission. Once the LMXRBs are removed, there are galaxies with hardly any hot gas, suggestive that galactic winds are occurring. Also, the  $L_X$  to  $L_B$  relationship has less scatter without the binaries, but there is still a large range in  $L_X$  at fixed  $L_B$ , suggesting that winds may be more forceful in some galaxies than others. The gas temperature is hotter than the stellar velocity dispersion, also consistent with an additional heat source, such as supernovae. The Fe abundance of the gas is near-solar but the O abundance is sub-solar, consistent with the metallicities of the old stellar population that fills these ellipticals. We can determine the rate at which the gas is cooling by measuring the OVI line intensity with FUSE (sensitive to gas at  $3 \times 10^5$  K), and about one-third of the 18 galaxies observed show this emission. The detected galaxies are generally optically bright and X-ray luminous, as would be expected and the cooling rate is a little less than the stellar mass loss rate, but the FUSE spectrograph only observes part of the galaxy. Finally, emission lines are detected from cooled gas ( $10^4$  K), which appears to have the same metallicity as the X-ray emitting gas and the stars. Therefore, for ellipticals, one can make a good case that the cooling flow picture is successful, if modified by galactic winds. The primary problem with this result is that fewer young stars are present than would be expected if the cooling gas were to form stars with a normal initial mass function.

### 1. Introduction

Unlike the cluster cooling flow case, where major revisions have been proposed to the basic model, there is mounting evidence that some of the original aspects of cooling flows occur in elliptical galaxies. To begin, the model of cooling flow ellipticals posits that gas is shed by stars and this gas becomes thermalized (heated to the velocity dispersion of the stars), and probably heated further by infrequent Type I supernovae that occur in these systems. If the gas remains bound to the galaxy, it cools and flows inward, eventually producing cooled gas that forms into stars. If the heating by supernovae is sufficient to raise the gas temperature above the escape temperature, it flows outward as a galactic wind, which produces only weak X-ray emission, in contrast to the case where the gas is bound. The general goal of the field is to find evidence for as many parts of this scenario as possible and to identify areas of problems or conflicts. Along these lines, I will try to review progress in this area,

which has been the primary goal of a multi-wavelength thesis (Athey 2003).

### 2. Mass Loss from Stars

Definitively determining the origin of the hot interstellar medium (ISM) in early-type galaxies provides critical information in evaluating the validity of the galactic cooling flow model. While the traditional model has the hot ISM originating from stellar mass loss, this presumption has been called into question by the numerous claims of substantially sub-solar metallicities from measurements of the X-ray emitting gas with previous generations of X-ray satellites (e.g., Matsumoto et al. 1997; Matsushita et al. 2000; Buote & Fabian 1998). The sub-solar metallicity of the hot ISM challenges the cooling flow model as the stars that shed this material have measured metallicities of solar and super-solar from integrated spectral synthesis modeling (e.g., Trager et al. 2000a,b; Terlevich & Forbes 2002). A direct observation of the galactic-wide

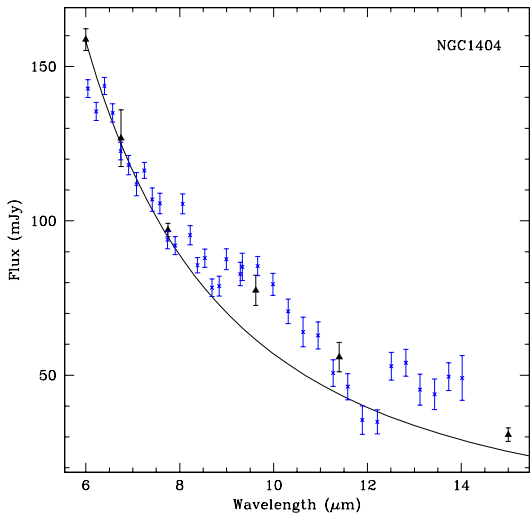


FIG. 1.— Galaxy NGC 1404 spectral energy distribution from CAM and CVF data with a blackbody fit. Emission feature at  $9.7\mu\text{m}$  is consistent with oxygen-rich AGB silicon dust feature seen in many nearby AGB stars. Filled triangles represent the narrow-band LW4-9 flux determinations and the “x”es illustrate the CVF measurements.

stellar mass loss rate (and consequently ISM injection rate) provides a key piece of information with which to evaluate the cooling flow model.

The mass loss from an ensemble of old stars is based upon well established models of stellar evolution, however direct evidence of this process had been lacking until the launch of the infrared space observatories, *The Infrared Astronomical Satellite (IRAS)* and *The Infrared Satellite Observatory (ISO)*. Stellar mass loss includes not only the outflow of gas, but the condensation of dust out of this gas, which forms a shell at a few to ten stellar radii from the dying star (for a review see Habing 1996). This shell absorbs radiation from the star and the silicates in the cloud will re-radiate in the  $9\text{--}15\mu\text{m}$  region which has been observed in individual giant stars in the Milky Way and the Magellanic Clouds (e.g., Whitelock et al. 1994; van Loon et al. 1999). However, the emission from individual stars is much too faint to be detected at the distance of nearby normal elliptical galaxies (e.g., in Virgo), but the emission from an ensemble of mass-losing stars in an elliptical is just detectable with *IRAS* (Knapp et al. 1992) and can be explored in detail with *ISO*.

The signature for mass loss from stars is a mid-IR excess near  $10\mu\text{m}$ , which we searched for by imaging a sample of nine elliptical galaxies with six medium band filters from  $6\text{--}15\mu\text{m}$ , along with one higher resolution spectrum in the same spectral region (Athey et al. 2002). The emission from  $6\text{--}8\mu\text{m}$  is just the stellar continuum from the galaxy and, as expected, it has the shape of the Rayleigh-Jeans spectrum (Fig. 1). However, compared to non-mass losing stars (or a Rayleigh-Jeans profile), the spectrum has additional emission at wavelengths longer than  $9\mu\text{m}$ , which is exactly where one would expect from stellar mass loss in giant stars. Whereas the six medium band measurements permit one to measure the

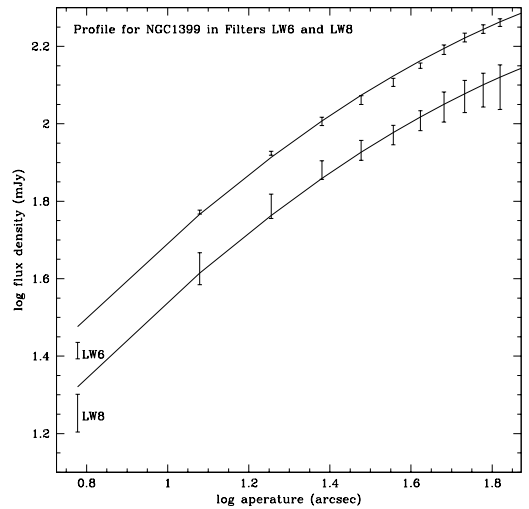


FIG. 2.— Surface brightness profiles plotted with de Vaucouleurs’  $R^{1/4}$  law fits. K and M starlight is traced in the LW6 band,  $7.00\text{--}8.50\mu\text{m}$ . Dust in addition to starlight is traced in the LW8 band,  $10.7\text{--}12.0\mu\text{m}$ . The agreement between the model and the data in both the LW6 and LW8 band shows that the dust is distributed throughout the galaxy in the same manner as the stars.

excess emission, higher spectral resolution is necessary to demonstrate that it has the same spectrum as the nearby mass-losing giants in the Milky Way. The spectrum of one target, NGC 1404, was obtained at improved resolution with the Circular Variable Filter on *ISO-Cam*, which gives  $\Delta\lambda \approx 0.3\mu$  instead of  $\Delta\lambda \approx 1\mu$ . This spectrum is well characterized from known Galactic mass losing stars such as *gHer* and confirms that the mid-IR excess represents a detection of the ensemble of mass losing stars in these galaxies.

Another expectation is that the mass loss rate should follow the stellar light distribution since the mass losing stars are an evenly distributed subset of the full stellar population. This was tested within the field of view of the *ISO-Cam*, about  $3.2'$  with  $6''$  pixels. The radial property of the mid-IR emission is consistent with a de Vaucouleurs profile, confirmation that this is associated with the average stellar population.

The mid-IR excess can be converted into a mass-loss rate, given a ratio of luminosity to mass loss, which can be determined for individual stars. Unfortunately, this ratio depends upon metallicity and the gas-to-dust ratio, so we used ratios that are inferred from both Galactic stars and Magellanic Cloud stars. Also, we are only observing part of these galaxies with *ISO*, so we corrected for the fraction of the galaxy not observed (typically  $\sim 1/2$ ). The final inferred mass loss rates were  $0.1\text{--}1.0 M_{\odot} \text{ yr}^{-1}$ , which is consistent with the theoretical estimates. In order to improve upon this result, we would need both more accurate measurements of the mid-IR excess as well as a more accurate value of the conversion ratio, which will probably become available from future *SIRTF* studies.

To summarize, these *ISO* observations confirm the expectation of the rate of gas that is entering these galaxies

and that there are metals in the gas, some of which is locked into grains. This stellar mass loss will eventually be spread throughout the galaxy, in which case it would be much colder (20-30 K) and could be detected in the far-IR region. However, the *ISO-Phot* instrument had poorer sensitivity than expected, so this faint emission was not detected (Temi et al. 2003).

### 3. An X-ray Survey With Chandra

There have been X-ray surveys of early-type galaxies starting with the *Einstein Observatory*, and each of these studies have led to an advance in the field. The most comprehensive previous study has been carried out with *ROSAT* (O’Sullivan et al. 2001), although there have been other focused studies (e.g., Davis & White 1996; Brown & Bregman 2000; O’Sullivan et al. 2003). These works show that the relationship between the X-ray and optical properties,  $\log L_X = m \log L_B$ , has  $m = 2.2$ – $4.0$ , depending on what is assumed for the stellar contribution. However, this relationship has a great deal of scatter and is not well-suited to a single power-law fit. Therefore, one of the controversial issues is how one deals with the X-ray binary contribution, and the removal of this contribution affects not only the luminosity, but the temperature and metallicity as well. A great advantage of *Chandra* is that it permits one to remove the point source contribution and analyze the X-ray emission from gas directly. Although the nature of the X-ray binaries in these galaxies is an area of considerable interest (Angelini et al. 2001; Blanton et al. 2001; Irwin et al. 2003), I will concentrate on the emission from the gas and its relationship to cooling flows. This *Chandra* sample of 37 early-type galaxies is discussed by Athey (2003).

First, one must isolate the gas emission by removing the contribution of the binaries. Previously this was accomplished by removing a mean value that is proportional to the optical luminosity, since the spatial resolution of earlier satellite mission was insufficient to resolve this point source emission. We find that there is considerable variation in the ratio  $L_{XRB}/L_B$  (a range of more than an order of magnitude), so although it has a mean value of  $\log L_{XRB}/L_B = 29.97 \pm 0.37$  (where  $L_{XRB}$  is in  $\text{erg sec}^{-1}$  and  $L_B$  is in  $L_\odot$ ), it is essential to remove this component from each galaxy separately if one is going to accurately determine gas masses, temperatures, metallicities, and other quantities.

Some of us had expected that once the X-ray binary contribution was removed, the  $L_{X,gas}$  to  $L_B$  relationship would converge and become well defined, but this is not the case. The range of  $L_{X,gas}$  at fixed  $L_B$  is still substantial (Fig. 3). Excluding the two dwarf galaxies from the fit, the slope is about 3.3, which is steeper than the nominal theoretical predictions, which range from  $3/2$ – $5/2$ . The steeper slope is most likely due to the presence of galactic winds, that are probably present in the lower luminosity systems (David et al. 1991). We note that the brightest cluster galaxies, usually at the centers of groups or clusters, are brighter than the average galaxy both in  $L_B$  and  $L_X$  (as has been first noticed by Helsdon et al. 2001; O’Sullivan et al. 2001) and this modifies the relationship, although not greatly.

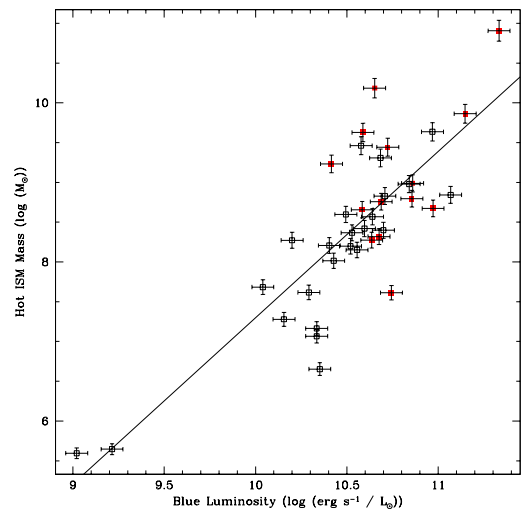


FIG. 3.— The hot ISM mass detected within the *Chandra* ACIS-S3 pointing is plotted as a function of blue luminosity. Filled symbols are BGG objects. The mass of the ISM is seen to increase more quickly than the mass of the stars. The solid line is the best fit slope of  $2.09 \pm 0.63$ .

The existence of galactic winds make a few predictions that can be tested: the gas temperature should be near the escape temperature; and the gas mass should be consistent with that expected from winds. First, we should note that there is a lower limit on the mass of gas that should be present in a galaxy with a galactic wind. This minimum mass is the product of the mass loss rate and the flow time for the wind, which is  $\sim 10^8$  yr for typical, nearby galaxies (within  $R_e$ ). The mass loss rates within this region are typically  $0.1$ – $1.0 M_\odot \text{ yr}^{-1}$ , so the minimum mass is  $10^7$ – $10^8 M_\odot$ , and if the galaxy has a partial wind (gas retained within a stagnation radius) rather than a complete wind, the expected mass will be higher (we exclude the two dwarf galaxies in this discussion). The gas masses of the galaxies with relatively low X-ray luminosities (the best galactic wind candidates) have masses as low as about  $10^7 M_\odot$  (Fig. 3), consistent with this expectation.

Galactic winds are driven by supernova heating since the SNR raise the temperature of the gas above the initial thermalization of the stellar mass loss, which is equal to the velocity dispersion temperature. For the high mass galaxies with deep potential wells, this increase in temperature is usually not enough to render the gas unbound, unlike the lower mass systems. The escape temperature is approximately twice the velocity dispersion temperature, so we examine the relationship between  $T_X$  and  $T_\sigma$  (the stellar velocity dispersion temperature; Fig. 4) and find that the gas temperature is usually hotter than  $T_\sigma$  (first shown by Davis & White 1996), and for the galaxies with relatively less mass, it is often about twice  $T_\sigma$ , as one would expect for a galactic wind. These two sets of observations support the suggestion that galactic winds are present in the galaxies with low  $L_{X,gas}/L_B$  ratios and that this process is important

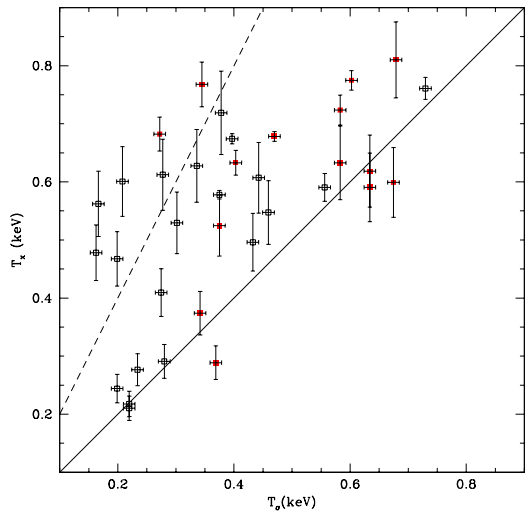


FIG. 4.— Gas temperature is plotted against stellar kinetic temperature. BGG objects are represented by filled symbols. The stellar kinetic temperature is calculated from velocity dispersions listed in McElroy (1995). A line representing equal gas and stellar temperatures is depicted as a solid line. Gas with temperatures greater than twice the stellar temperature are hotter than the implied escape velocity. Galaxies in this regime are found above the dashed line.

in shaping the  $L_{X,gas}$  to  $L_B$  relationship.

The radial distribution for the gas is still fit by a  $\beta$  model with  $\beta \approx 0.5$ , as found previously by O’Sullivan et al. (2001), but there is little correlation between the core radius, as defined by the X-ray emission, and the optical  $R_e$ , as had been suggested by previous works. For some galaxies, the core radius is so small that it is unresolved by *Chandra*, so the surface brightness distribution is a power-law right into the center.

One of the other new contributions by the survey with *Chandra* is the measurement of the metallicities, a controversial area in which previous studies found variation by a factor of several, depending upon how the analysis was carried out. The two problems facing investigators were the issue of dealing with the X-ray binaries, and spectral resolution that was inadequate to separate the different metal features. The measurement of the metals is also sensitive to calibration issues, which often are more problematic in the soft end of the detector, which is where many of the best lines lie. With the recent calibration corrections for *Chandra*, the instrument should be capable of obtaining good metallicities for oxygen, iron, silicon, and magnesium, at least for observations with an adequate number of photons. We show a typical good example of the results for NGC 5044 (Fig 5), where the oxygen metallicity is about 1/4 of the solar value, the iron metallicity is about  $0.6 Z_\odot$ , while the abundances of Si and Mg are about solar (relative to the solar photospheric abundances of Anders & Grevesse 1989). Our derived metallicities are confirmed by the much higher resolution *XMM-Newton* Reflection Grating Spectrometer data for common galaxy observations (Xu et al. 2002; Tamura et al. 2003). These metallicities are a bit lower

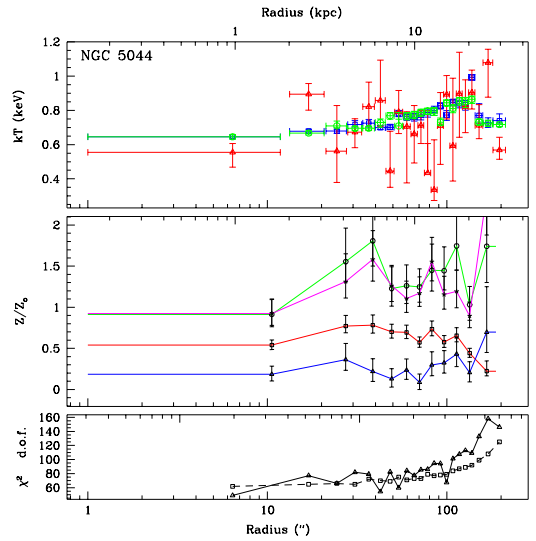


FIG. 5.— Temperature and Metallicity Profile for NGC 5044. All Panels show radius in arcseconds on the lower x-axis and radius in kiloparsecs on the upper x-axis. The top panel displays temperature determinations with squares representing an on-chip, outer region background, circles representing a blank sky background, and triangles representing a deprojection background (See Athey (2003) for full descriptions of these backgrounds.) The middle panel displays metallicity information with all metals relative to solar photospheric abundances as reported in Anders & Grevesse (1989). In the middle panel iron abundance is represented as a square, oxygen abundances is represented as a circle, and silicon abundances is represented as a star. The data in the middle panel are determined from an on-chip outer region background. The bottom panel displays the statistical characterization of the model fits to the data from the on-chip, outer region background. Typically, the model fits with the blank sky background display similar behavior. The number of degrees of freedom are represented by squares and the triangles represent chi-squared.

than the stellar abundance measurements for Fe, but the stellar measurements sample the center while the abundances in the hot gas encompasses a region typically 10 kpc in radius. As ellipticals have abundance gradients, it would not be surprising to obtain lower abundances from a region that extends further in radius. Finally the stellar spectral synthesis has a zero point uncertainty of a factor of about two, although the relative precisions are much more accurate.

The ratios of the metal abundances are far from the values that are found for the cold gas in the Milky Way, but they are similar to expectations for an old population. The abundances in the gas result from a combination of Type Ia supernovae (the only type known to occur in normal ellipticals) and the abundances of the underlying stellar population that is losing mass. The Type Ia should dominate the Fe content, and as these supernovae produce only modest amounts of O, the Fe/O ratio should be greater than unity. We find that the abundance ratios can be fit with a combination of 80% of the yield from Type Ia supernovae and 20% of the yield from Type II supernovae.

Finally, we briefly examine the entropy and density distributions for NGC 5044 as a typical example (Fig. 6),

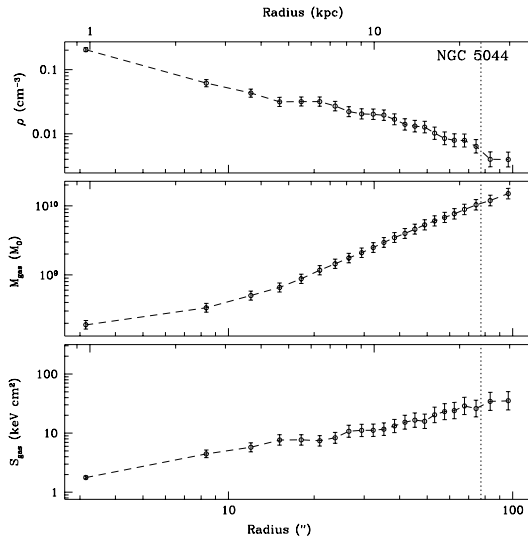


FIG. 6.— Density, Mass and Entropy Profile for NGC 5044. All Panels show radius in arcseconds on the lower x-axis and radius in kiloparsecs on the upper x-axis. The vertical dotted line shows the optical half-light radius. The top panel displays electron density. The middle panel displays the cumulative mass profile in solar units. The bottom panel displays the entropy of the gas in units of  $\text{keV cm}^2$ .

where we can extend the work from the *ROSAT* studies (O’Sullivan et al. 2003) into smaller radii. One finds that the central density often exceeds  $0.1 \text{ cm}^{-3}$  in the inner kpc, which pushes the cooling time below  $10^{7.5} \text{ yr}$ . The entropy gradient also continues into the central region. As such a gradient would be eliminated if there were significant large-scale turbulence in the galaxy, the gas motions must be relatively modest (i.e., the turbulent velocity, on the scale of  $R_e$ , would need to be well below the sound speed).

#### 4. An OVI Survey With *FUSE*

If gas is cooling below the ambient temperature of the X-ray emitting gas, it will pass through the region in which OVI is present, in the  $1\text{--}10 \times 10^5 \text{ K}$  region. In this temperature range, and in particular, near  $3 \times 10^5 \text{ K}$ , OVI is the primary coolant, so the luminosity in the OVI line is a direct measure of the rate at which gas is cooling. The OVI ion has two strong transitions at  $1032 \text{ \AA}$  and  $1038 \text{ \AA}$ , which are the primary cooling lines and although they fall outside of the range of *HST*, they are accessible to the *Far Ultraviolet Explorer (FUSE)*, a high-resolution spectroscopic telescope that operates in the  $910\text{--}1180 \text{ \AA}$  range and it has a large aperture ( $30''$  square) that can take in the inner part of an early-type galaxy. Using *FUSE*, we are in the process of completing a set of observations of a complete sample of optically selected normal early-type galaxies. As these are the optically brightest 18 galaxies, they include many of the famous X-ray bright systems as well as a number of galaxies with relatively low X-ray luminosities.

Observations of NGC 1404 and NGC 4636 are already published (Bregman et al. 2001b), and although no OVI was detected from NGC 1404, these lines were detected

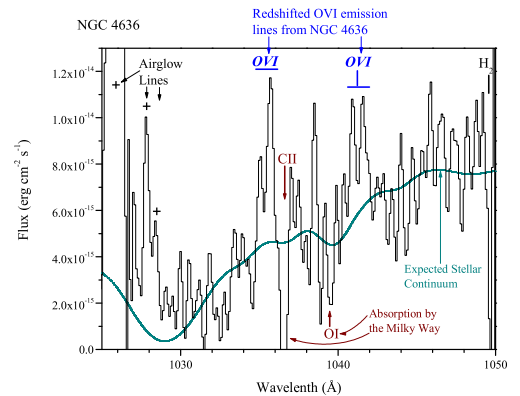


FIG. 7.— The *FUSE* Spectra of NGC 4636 contains a stellar continuum, with a dotted line model fit, Galactic absorption lines from low ionization species, airglow lines, plus OVI emission lines at the redshift of the galaxy. The OVI emission line signifies the presence of cooling gas at about the rate predicted from the cooling flow model.

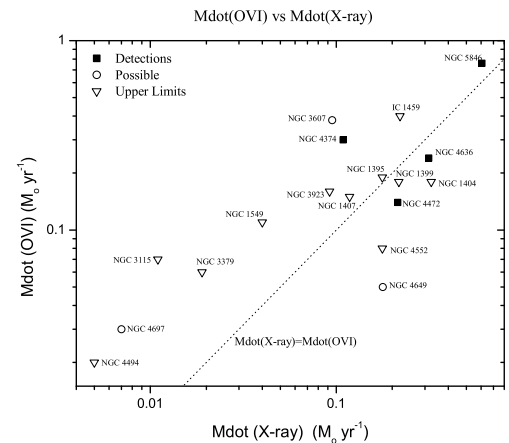


FIG. 8.— The OVI emission line luminosity measured by *FUSE*, expressed in units of  $M_{\odot} \text{ yr}^{-1}$ , vs the X-ray cooling rate inferred from *ROSAT* data for 18 galaxies in our sample. The X-ray poor galaxies are not detected in OVI while several of the X-ray bright ones are detected, consistent with the picture that the X-ray poor galaxies have galactic winds while the X-ray bright galaxies have cooling flows.

from NGC 4636 (Fig. 7). The luminosity of these lines corresponds to a cooling rate of  $0.4 M_{\odot} \text{ yr}^{-1}$ , which is less than the total rate from the cooling flow model of about  $2 M_{\odot} \text{ yr}^{-1}$ , but the *FUSE* aperture only takes in a part of the galaxy. The amount of cooling mass that is produced within the *FUSE* aperture is model dependent and for models with distributed mass drop out (e.g., the  $q = 1$  model of Sarazin & Ashe 1989), the prediction equals the observation. This would subsequently predict that the OVI emission is extended in the galaxy, which we do not observe, but our limits are not particularly restrictive.

For the larger sample (Bregman et al. 2001a), we detect OVI emission clearly from five of 18 galaxies and possibly

from two others in the sample (Fig. 8). All five detections are of galaxies that are massive or have relatively high X-ray luminosities: NGC 1316, NGC 4374, NGC 4472, NGC 4636, and NGC 5846. These are the types of galaxies that are expected to retain their gas, which should cool. The cooling rates inferred from the OVI lines are similar to the values predicted within the 30" aperture for the distributed cooling model. Also, none of the low optical luminosity galaxies or those with relatively low X-ray luminosities are clearly detected. None were predicted to be detected as they have partial or total galactic winds, so that the rate of cooling gas is below our detection threshold (generally about  $0.1 M_{\odot} \text{ yr}^{-1}$ ).

There are a few unexpected results and a several remaining questions regarding this sample. Some of the X-ray bright galaxies were not detected, with upper limits about a factor of two below the expected value (NGC 1399 and NGC 1404). One other X-ray bright galaxy is undetected (NGC 4552) but its X-ray emitting gas mass is 2–10 times lower than that of the detected sources, so it will be necessary in the future to take into account the gas mass and not just the cooling rate derived from  $L_X$  (some galaxies observed by *FUSE* do not yet have *Chandra* observations, so we used the *ROSAT* data for the initial analysis). Despite these minor issues, the OVI detections support the basic cooling flow predictions for the rate of cooling gas, to within a factor of two. Unfortunately, the predicted OVI line luminosities are only weakly dependent on metallicity, so we gain no metallicity information, except that we know that the metallicity is not extremely low.

### 5. The Metallicity of the Cool Gas

One of the last stages of this picture should be the presence of gas below  $10^4 \text{ K}$  and the search for warm ionized gas ( $3\text{--}10 \times 10^4 \text{ K}$ ) has been quite successful (e.g., Trinchieri & di Serego Alighieri 1991; Goudfrooij et al. 1994; Macchetto et al. 1996), while the search for neutral atomic gas and molecular gas has had fewer successes (Gallagher et al. 1975; Faber & Gallagher 1976). Evidently, if the gas is passing through this temperature range on the way to becoming stars, it does so rapidly ( $< 10^{8.5} \text{ yr}$  for neutral and molecular gas;  $\sim 10^6 \text{ yr}$  for the warm ionized component). This is not a real problem as the observed masses (or upper limits) are greater than the masses predicted by the product of the X-ray cooling rate and the radiative cooling time for gas in pressure equilibrium with its surroundings. So although the detected masses are not strong constraints on the model, the metallicity and spatial distribution are.

One might expect that the spatial distribution of the warm ionized gas indicates the location of the cooling gas, which bears on the issue of distributed cooling. Most of the galaxies detected in the optical emission lines (e.g.,  $\text{H}\alpha$ ) are measured in the central region (about 30"), but this may simply be a detection threshold limitation. The structure of the  $\text{H}\alpha$  emitting gas appears to be related to structure in the X-ray emitting gas, suggesting a connection between them (Trinchieri et al. 1997; Trinchieri & Goudfrooij 2002). In the most warm-gas rich galaxies, the velocities in the  $\text{H}\alpha$  gas are much greater than the

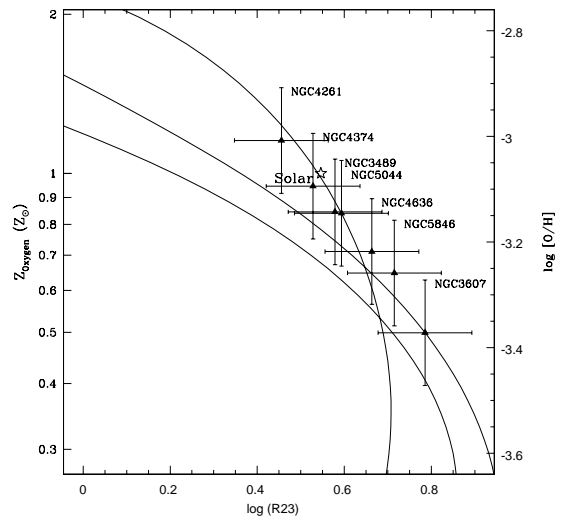


FIG. 9.— R23 Diagram. Solar metallicity is represented as a star. Different ionization parameters are shown as solid lines. Errors are 0.2 dex as indicated by the intrinsic uncertainties of the R23 method applied to a global galaxy spectra (Kobulnicky et al. 1999).

stellar rotational velocities, but are comparable to infall or rotational velocities ( $100\text{--}200 \text{ km sec}^{-1}$ ; Caon et al. 2000). From the velocities, it is not possible to distinguish between cooling flow material that is falling and/or rotating within the galaxy in a complex fashion (e.g., in NGC 4636) and material that has been captured from some other galaxy.

Two distinct but plausible origins for the warm ISM can be distinguished by the metallicity of the gas, as the stellar population shedding material into the ISM has measured metallicity of solar and above (e.g., Trager et al. 2000b,a; Terlevich & Forbes 2002) while the cluster or group medium is about 1/3 of the solar value. One potential complication is that the stellar metallicity decreases with radius, (and it is not well-measured beyond  $R_e$ ; the inner few kpc), so it may be difficult to distinguish between stellar mass loss and accretion in the outer part of the galaxy. However, in the inner region, the distinction by metallicity should be clear.

We obtained spectra of a number of early-type galaxies and measured the OII and OIII line strengths (as well as NII,  $\text{H}\alpha$ ,  $\text{H}\beta$ , and SII) and determined oxygen abundances for the warm ionized gas in the central region of seven galaxies. These oxygen abundances are generally in the  $0.6\text{--}1.0 Z_{\odot}$  range (Fig. 9), which is similar to the metallicity of the stars in these galaxies. It is about a factor of 2-3 times larger than the oxygen abundances measured in the X-ray emitting gas. It is unclear if this is a problem, as the abundances in the X-ray gas are determined over a significantly larger region and the abundances often rise into the central region. The observations do rule out the possibility that the majority of the warm ionized gas is material captured from a dwarf galaxy, and it may be consistent with having come from a cooling flow.

## 6. Final Comments

Many aspects of the basic cooling flow and galactic wind picture seems to be verified by observations. The mass loss from the stars is directly detected and the metallicity of the hot X-ray emitting gas is similar to that expected from an old stellar population. The galaxies with relatively little hot gas mass are generally the lower luminosity galaxies that do not reside in cluster or group centers and they have shallower potential wells than the more massive galaxies. These lower mass galaxies are probably driving galactic winds, so little gas is retained to cool. Of these X-ray poor galaxies, they are hardly ever detected in the OVI emission line, a tracer of cooling gas (and cooling flows). In contrast, the more massive galaxies retain more hot gas and they often show OVI emission line gas at about the level predicted from cooling flows. Furthermore, the warm ionized gas has a metallicity that is similar to the stars and consistent with having come from a cooling flow, provided that the metallicity gradient extends into the central 30" of the galaxy.

There are a few shortcomings to this picture that are not yet understood. In NGC 4636, emission from the OVIII line is seen in the X-ray observations with *XMM-Newton* (Xu et al. 2002). Those same observations fail to detect much emission from OVII, which would be indicative of cooling gas, but emission from the OVI line is detected by *FUSE*. We don't really understand how a system can produce OVIII and OVI, but not OVII unless

there is mixing of the gas with cool material that causes it to quickly go from 0.5 keV to below 0.1 keV (the temperature in which OVII would be present; see the mixing model of Fabian et al. 2002).

The other concern is the lack of young stars in these galaxies. If the end result of the cooling flow systems are stars that are made with a normal initial mass function, one should see evidence of the hot young stars that are formed. Spectroscopically, O and B stars have strong C IV absorption (1550 Å) that is not detected by O'Connell (1999) and although their spectral resolution is poor, they are able to place limits on the rate of normal star formation significantly less than  $0.1 M_{\odot} \text{ yr}^{-1}$ , whereas the OVI emission infers rates of at least  $0.1\text{--}0.6 M_{\odot} \text{ yr}^{-1}$ . One explanation could be that star formation does occur but that the initial mass function of star formation is truncated at less than  $1.0 M_{\odot}$  (O'Connell 1999). However, star formation that occurs in the inner part of a galaxy for an extended period may change the optically observed properties, making it inconsistent with observations (Mathews 1988). We hope that by the next meeting on this subject, there will be a resolution to these problems.

We would like to acknowledge support for this work from NASA grants NAG5-11483, G01-2089X, G01-2087X, and NAG5-10765.

## References

- Anders, E. & Grevesse, N. 1989, *Geochim. Cosmochim. Acta*, 53, 197
- Angelini, L., Loewenstein, M., & Mushotzky, R. F. 2001, *ApJ*, 557, L35
- Athey, A. 2003, PhD thesis, University of Michigan
- Athey, A., Bregman, J. N., Bregman, J. D., Temi, P., & Sauvage, M. 2002, *ApJ*, 571, 272
- Blanton, E. L., Sarazin, C. L., & Irwin, J. A. 2001, *ApJ*, 552, 106
- Bregman, J. N., Miller, E., & Irwin, J. A. 2001a, *Bulletin of the American Astronomical Society*, 33, 1339
- Bregman, J. N., Miller, E. D., & Irwin, J. A. 2001b, *ApJ*, 553, L125
- Brown, B. A. & Bregman, J. N. 2000, *ApJ*, 539, 592
- Buote, D. A. & Fabian, A. C. 1998, *MNRAS*, 296, 977
- Caon, N., Macchetto, D., & Pastoriza, M. 2000, *ApJS*, 127, 39
- David, L. P., Forman, W., & Jones, C. 1991, *ApJ*, 380, 39
- Davis, D. S. & White, R. E. 1996, *ApJ*, 470, L35
- Faber, S. M. & Gallagher, J. S. 1976, *ApJ*, 204, 365
- Fabian, A. C., Voigt, L. M., & Morris, R. G. 2002, *MNRAS*, 335, L71
- Gallagher, J. S., Faber, S. M., & Balick, B. 1975, *ApJ*, 202, 7
- Goudfrooij, P., Hansen, L., Jorgensen, H. E., & Norgaard-Nielsen, H. U. 1994, *A&AS*, 105, 341
- Habing, H. J. 1996, *A&A Rev.*, 7, 97
- Helsdon, S. F., Ponman, T. J., O'Sullivan, E., & Forbes, D. A. 2001, *MNRAS*, 325, 693
- Irwin, J. A., Athey, A. E., & Bregman, J. N. 2003, *ApJ*, 587, 356
- Knapp, G. R., Gunn, J. E., & Wynn-Williams, C. G. 1992, *ApJ*, 399, 76
- Kobulnicky, H. A., Kennicutt, R. C., & Pizagno, J. L. 1999, *ApJ*, 514, 544
- Macchetto, F., Pastoriza, M., Caon, N., Sparks, W. B., Giavalisco, M., Bender, R., & Capaccioli, M. 1996, *A&AS*, 120, 463
- Mathews, W. G. 1988, *AJ*, 95, 1047
- Matsumoto, H., Koyama, K., Awaki, H., Tsuru, T., Loewenstein, M., & Matsushita, K. 1997, *ApJ*, 482, 133
- Matsushita, K., Ohashi, T., & Makishima, K. 2000, *PASJ*, 52, 685
- McElroy, D. B. 1995, *ApJS*, 100, 105
- O'Connell, R. W. 1999, *ARA&A*, 37, 603
- O'Sullivan, E., Forbes, D. A., & Ponman, T. J. 2001, *MNRAS*, 328, 461
- O'Sullivan, E., Ponman, T. J., & Collins, R. S. 2003, *MNRAS*, 340, 1375
- Sarazin, C. L. & Ashe, G. A. 1989, *ApJ*, 345, 22
- Tamura, T., Kaastra, J. S., Makishima, K., & Takahashi, I. 2003, *A&A*, 399, 497
- Temi, P., Mathews, W. G., Brighenti, F., & Bregman, J. D. 2003, *ApJ*, 585, L121
- Terlevich, A. I. & Forbes, D. A. 2002, *MNRAS*, 330, 547
- Trager, S. C., Faber, S. M., Worthey, G., & González, J. J. 2000a, *AJ*, 120, 165
- . 2000b, *AJ*, 119, 1645
- Trinchieri, G. & di Serego Alighieri, S. 1991, *AJ*, 101, 1647
- Trinchieri, G. & Goudfrooij, P. 2002, *A&A*, 386, 472
- Trinchieri, G., Noris, L., & di Serego Alighieri, S. 1997, *A&A*, 326, 565
- van Loon, J. T., Groenewegen, M. A. T., de Koter, A., Trams, N. R., Waters, L. B. F. M., Zijlstra, A. A., Whitelock, P. A., & Loup, C. 1999, *A&A*, 351, 559
- Whitelock, P., Menzies, J., Feast, M., Marang, F., Carter, B., Roberts, G., Catchpole, R., & Chapman, J. 1994, *MNRAS*, 267, 711
- Xu, H., Kahn, S. M., Peterson, J. R., Behar, E., Paerels, F. B. S., Mushotzky, R. F., Jernigan, J. G., Brinkman, A. C., & Makishima, K. 2002, *ApJ*, 579, 600